

26 . TRACE-ELEMENT CHARACTERISTICS OF LEG 61 BASALTS¹

Rodey Batiza, Department of Earth and Planetary Sciences, McDonnell Center for the Space Sciences, Washington University, St. Louis, Missouri

ABSTRACT

Basalts from Leg 61 have trace-element characteristics similar to those of fresh basalts from active mid-ocean ridges. The lower basalt flows exhibit coherent chemical-stratigraphic variations trends, as do the upper series of sills. A single 50-meter-thick sill exhibits more complex variation in trace-element abundance. These chemical-stratigraphic trends are provisionally interpreted in terms of partial melting and fractionation differences of liquids produced from a mantle source similar to that of mid-ocean-ridge basalt (MORB). It has thus apparently been possible to produce basalts with MORB-type trace-element abundances in tectonic settings other than mid-ocean ridges.

INTRODUCTION

Drilling during DSDP/IPOD Leg 61 at Site 462 penetrated over 500 meters of basaltic igneous rock. The macroscopic aspects of these sills and flows, their stratigraphy, mineralogy, alteration, bulk chemical composition, and isotopic composition are discussed in Batiza et al. (this volume), in the Site Summary, and in other chapters of this volume. Broadly, the igneous complex consists of two parts: (1) a lower section (348.5 m penetrated), of unknown total thickness, consisting of thin and thick sheet flows or submarine pahoehoe units, and (2) an upper unit (155 m thick) of zeolitic volcanoclastic sediments intruded by basalt sills ranging from a few centimeters to 50 meters in thickness (see Fig. 1). The purpose of this article is to present trace-element data for the igneous complex. I give 7 analyses of material from the pilot hole (462) and 31 analyses of material from the multiple re-entry hole (462A), as well as 2 new analyses of basalt from the Ontong-Java plateau, drilled during Leg 30 at Site 289 (see Table 1). Analyses of samples from the bottom 100 meters or so of Hole 462A are given by Seifert (this volume).

EXPERIMENTAL METHODS

Trace-element analyses were carried out using the instrumental neutron-activation analysis (INAA) methods described by Jacobs et al. (1977). Analytical precision for La, Ce, Sm, Eu, Tb, Co, Sc, Th, and Cr is better than $\pm 5\%$. Precision for Yb is $\pm 7.6\%$, for Lu $\pm 14.4\%$, and for Hf $\pm 11.6\%$. Precision for Ni, Zn, Sr, U, Zr, and Rb is not precisely known, but comparisons with rocks analyzed by other methods suggest that abundances of trace elements can be determined to within $\pm 15\%$.

Analyses were carried out on splits or rock powder typically weighing about 100 mg. The rock powders were prepared by first crushing clean, dry rock slabs in a stainless steel Plattner mortar, then grinding them in an alumina canister in a shatter box. In general, except for a small thin-section chip, the entire sample from a given interval of core was sawed, washed, dried, and powdered. Nevertheless, sample sizes were usually smaller than desirable in order to avoid small-scale heterogeneity within the unit sampled: 20 to 60 grams total. Where possible, secondary vein material was avoided.

RESULTS

Table 1 gives trace-element abundance determinations for the samples analyzed. Partial major-element analyses by X-ray fluorescence methods aboard the *Glomar Challenger* are also listed. In most cases, the partial major-element analysis is not for exactly the same interval (and never for the same powder split) as the trace-element analyses. The major-element data are, however, always for samples from the same cooling unit, and were usually taken less than 10 cm away from samples analyzed for trace elements. Major-element data by wet chemical methods on 10 of the samples in Table 1 are given by Tokuyama and Batiza (this volume).

The abundances of rare-earth elements (REE) for representative samples are shown graphically on chondrite-normalized (Haskin et al, 1968) abundance diagrams in Figures 2 through 7. These figures show that most of the samples yield patterns similar to those for mid-ocean-ridge tholeiites. With only one exception, the Leg 61 basalts are depleted in light REE. Absolute abundances of REE are also very similar to those of mid-ocean-ridge tholeiite. This is true for other elements as well: Sc content ranges from 36 to 55 ppm; Cr 533 to 28 ppm; Ni 117 to 87 ppm (samples with less than about 80 ppm are below the detection limits for Ni); Sr 59 to 144 ppm; Zr 57 to 91 ppm (only 4 samples); and Na₂O is generally below 3.0 wt. %, usually below 2.5 wt. %. The low abundances of Sr, Zr, K, and light REE are, of course diagnostic of mid-ocean-ridge (Engel et al., 1965; Sun et al., 1979) tholeiitic basalts, and the high levels of Ni and Cr in some samples indicate that at least a few of the samples may have undergone only little fractionation and may be chemically similar to liquids derived from primary or at least parental mantle-derived liquids.

Stratigraphic Trends

The observed division between the lower section of flows and the upper section of sediment and sills occurs between Core 41 and Core 44 of Hole 462A. Igneous units from Core 44 downward are clearly flows, and ig-

¹ Initial Reports of the Deep Sea Drilling Project, Volume 61.

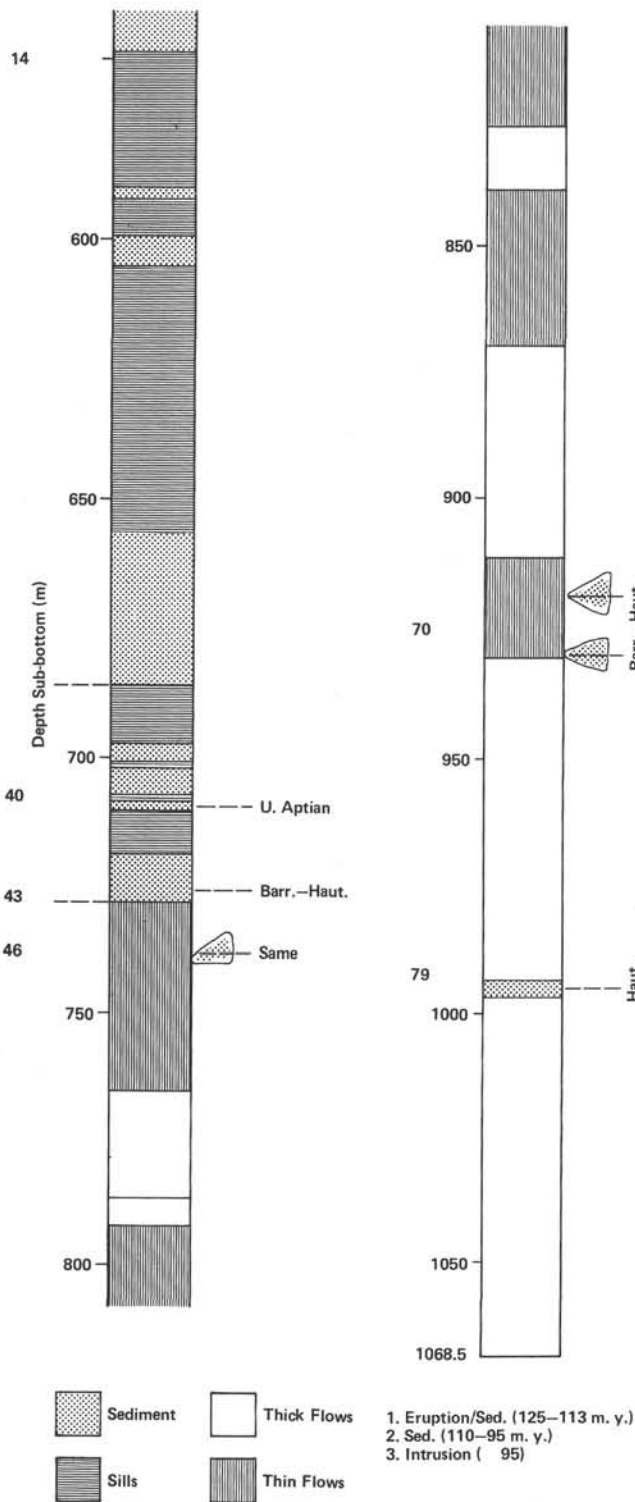


Figure 1. Generalized stratigraphy of Hole 462A, showing division between upper unit of sediments and sills and lower section of flows.

neous units above Core 41 are usually clearly identifiable as sills. Sediments at the bottom of Core 40 are upper Aptian, and those in Core 43 are thought to be Barremian. Thus, the stratigraphic division between flows and sills also corresponds to a depositional hiatus of from 5 to 20 m.y. Figure 8 shows that flows and sills

have different trace-element abundance patterns, with essentially no overlap. Volcanic Unit 21, located between the two dated sedimentary horizons, has very low total REE abundance, and occupies a pivotal position between two stratigraphic-chemical trends shown in Figure 9.

Figure 9 includes the data of Seifert (this volume), and shows that from the bottom of the hole upward, La and TiO₂ abundances and the FeO*/MgO ratio generally decrease through volcanic Unit 21, then increase again through the sills, although the data are much more scattered for the sills. Abundances of chromium increase and then decrease upward in the section, and thus show a pattern opposite to that of the stratigraphic variation of La, TiO₂, and FeO*/MgO ratio.

Variations within a Single Cooling Unit

Numerous samples from a single sill about 50 meters thick were analyzed to determine the extent of lateral and vertical chemical variation within the unit. Thin-section examinations of samples from this unit (Batiza et al., this volume) suggested considerable variability. The sill was penetrated by the pilot Hole 462 (Unit 11, Table 1) and also by the deep multiple re-entry Hole 462A (Unit 13). Ten samples of the sill were analyzed: 6 from Hole 462 and 4 from Hole 462A. Figures 2 and 3 show that, indeed, considerable chemical variation occurs within this thick sill; in fact, variation within this sill essentially defines the variation from the entire section of sills. The variation exhibits no simple stratigraphic pattern, and may be related to abundances of mobile late-stage liquid; but considerable detailed work remains to be completed before these variation patterns can confidently be interpreted.

DISCUSSION

I am deferring detailed interpretation of the trace-element data for Leg 61 basalts, for several reasons: (1) All the rocks are moderately to severely altered (see Batiza et al. and Windom and Book, this volume). (2) More trace-element and, especially, major-element analyses are needed before detailed interpretations can confidently be drawn.

Until the chemical effects of alteration of Leg 61 basalts are understood more fully, interpretations of the trace-element abundances must be cautious. Ludden and Thompson (1979) have shown that REE, for example, appear to fractionate during weathering of sea-floor basalts. This contrasts with the findings of Hellman et al. (1977), who show that REE may be mobile under certain low-temperature weathering or metamorphic conditions, but do not fractionate. Slight enrichment of Leg 61 basalts in the light REE during alteration could account for their apparent transitional MORB nature (Fig. 10).

Alternatively, Figure 10 could be interpreted to show that Leg 61 basalts have primary transitional MORB chemical affinities (Sun et al., 1979). This interpretation is provisionally to be preferred because of the close grouping of sills and flows and the coherence of major- and trace-element abundances of the Leg 61 rocks. The

chemical effects of alteration might be expected to result in a great deal of chemical variation, scatter, and lack of the usual observed coherent behavior of chemical elements, as shown by Ludden and Thompson (1979). Further, if the REE abundances in Leg 61 basalts are completely unaltered by sea-water weathering processes, it appears that, within the section of flows, transitional MORB affinities become more pronounced toward the top. The sills, on the other hand, appear to comprise a fractionated series very similar though not identical to many normal ridge-crest tholeiitic series. This is very interesting, since these basalts probably did not originate at mid-ocean ridge (Larsen and Schlanger, this volume).

These trends are associated with the stratigraphic-chemical trends described previously. A possible interpretation is that the trend exhibited by the section of flows—toward decreasing La and TiO₂ abundances and increasing Cr abundances upward in the section—may be due to an increase in the degree of partial melting, coupled perhaps with a gradual change in the nature of the mantle source toward a more transitional MORB-type mantle source. The trend exhibited by the sills, on the other hand, may result from the effects of shallow-level fractional crystallization. These interpretations are speculative at this point, and will no doubt be modified, perhaps greatly, when more complete data are available.

ACKNOWLEDGMENTS

I thank Larry Haskin and Marilyn Linstrom for making possible the trace-element analyses. This work supported in part by the National Science Foundation through DSDP/IPOD and NSF grant OCE7727001.

REFERENCES

- Engel, A. E. J., Engel, C. G., and Havens, R. G., 1965. Chemical characteristics of oceanic basalts and the upper mantle. *Geol. Soc. Am. Bull.*, 76:719-735.
- Haskin, L. A., Haskin, M. A., Frey, F. A., et al., 1968. Relative and absolute abundances of the rare earths. In Ahrens, L. H. (Ed.), *Origin and Distribution of the Elements*: New York (Pergamon Press), pp. 889-912.
- Hellman, P. L., Smith, R. E., and Henderson, P., 1977. Rare earth investigation of the Cliefden outcrop, N.S.W., Australia. *Contrib. Min. Petrol.*, 65:155.
- Jacobs, J. W., Korotev, R. L., Blanchard, D. P., et al., 1977. A well-tested procedure for instrumental neutron activation analysis of silicate rocks and minerals. *J. Radioanal. Chem.*, 40:93-114.
- Ludden, J. N., and Thompson, G., 1979. An evaluation of the behavior of rare earth elements during the weathering of sea-floor basalt. *Earth Planet. Sci. Lett.*, 43:85-92.
- Sun, S.-S., Nesbitt, R. W., and Shrawkin, A. Y., 1979. Geochemical characteristics of mid-ocean ridge basalts. *Earth Planet. Sci. Lett.*, 44:119-138.

Table 1. Trace-element and major-element data.

Element	Unit	10	11	11	11	11	11	11	1	2	4	7	9	12	12
Sample (interval in cm)		462-64-1, 8-11	462-66-1, 23-25	462-66-4, 16-20	462-66-5, 42-47	462-68-1, 67-71	462-68-2, 34-36	462-69-1, 20-24	462A-15-1, 66-68	462A-17-2, 84-86	462A-20-1, 115-121	462A-21-1, 140-143	462A-22-2, 120-124	462A-27-1, 94-97	462A-28-3, 1-2
La (ppm)		4.29	4.36	4.45	4.56	4.50	3.94	7.99	4.27	3.55	4.13	5.74	4.98	4.71	5.47
Ce (ppm)		13.12	10.73	12.60	12.82	12.39	10.02	20.52	10.82	9.24	11.53	15.36	14.26	12.77	14.86
Sm (ppm)		3.33	3.40	3.48	3.66	3.50	2.91	4.82	3.18	2.87	3.18	3.81	3.45	3.29	4.04
Eu (ppm)		1.29	1.16	1.23	1.21	1.24	1.09	1.58	1.18	1.03	1.11	1.47	1.35	1.17	1.36
Tb (ppm)		0.95	0.81	0.85	0.85	0.82	0.82	0.98	0.76	0.74	0.82	0.85	0.88	0.82	0.97
Yb (ppm)		3.78	3.06	3.23	3.29	3.33	2.98	3.94	2.87	2.74	2.98	3.33	2.26	3.15	3.68
Lu (ppm)		0.55	0.49	0.49	0.50	0.51	0.43	0.60	0.45	0.39	0.45	0.51	0.48	0.48	0.56
FeO (wt. %)		10.78	12.20	12.41	12.25	13.18	12.07	15.21	11.91	11.64	11.75	12.27	9.69	12.80	13.65
Sc (ppm)		51	44	46	45	46	46	44	47	48	41	51	55	45	46
Cr (ppm)		228	184	230	229	147	209	28	152	164	179	217	241	180	139
Co (ppm)		51	46	48	48	48	46	45	51	101	44	47	55	47	47
Ni (ppm)				98	87										
Zn (ppm)		40		123	65	164	36	153	138		114	161		141	120
Na ₂ O (wt. %)		2.63	2.27	2.31	2.27	2.26	2.15	3.04	2.47	2.22	1.99	2.87	2.98	2.29	2.46
Sr (ppm)			68	65	144				103			108	121	77	88
Hf (ppm)		2.96	2.57	2.67	2.79	2.71	2.42	3.31	2.47	2.24	2.51	3.04	3.35	2.57	3.05
Th (ppm)		0.41	0.32	0.34	0.42			0.31	0.23		0.25	0.35	0.36	0.31	0.40
U (ppm)															70
Zr (ppm)				91				57							
Rb (ppm)								8.4							
Sample (interval in cm)		462-64-1, 4-6	462-66-1, 19-21	462-66-4, 12-14		462-68-1, 73-75	462-68-2, 37-39	462-69-1, 36-38				462A-21-1, 146-149	462A-22-2, 111-115	462A-27-1, 97-100	462A-28-3, 8-10
SiO ₂ (wt. %)		49.4	49.6	49.5		49.8	50.2	48.3				47.8	49.8	49.4	48.9
TiO ₂ (wt. %)		1.91	1.64	1.64		1.85	1.92	2.13				1.88	2.08	1.52	1.37
Al ₂ O ₃ (wt. %)		15.53	13.36	13.64		12.96	12.70	12.01				15.06	16.78	13.39	13.69
FeO (wt. %)		10.78	12.64	12.31		13.80	14.33	16.79				12.88	11.25	12.77	12.17
MgO (wt. %)		7.52	6.72	7.24		6.55	6.30	5.47				6.30	7.47	6.70	6.66
CaO (wt. %)		10.05	11.14	11.08		10.52	10.17	9.32				8.99	7.60	11.14	11.86
K ₂ O (wt. %)		0.04	0.04	0.07		0.08	0.14	0.27				0.20	0.44	0.11	0.08

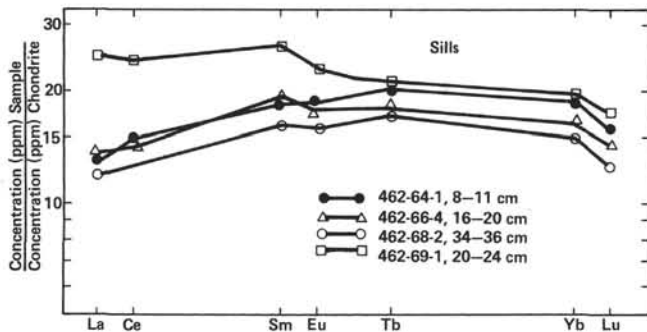


Figure 2. Chondrite-normalized (Haskin et al., 1968) REE abundances diagram for samples from thick sill at the bottom of Hole 462.

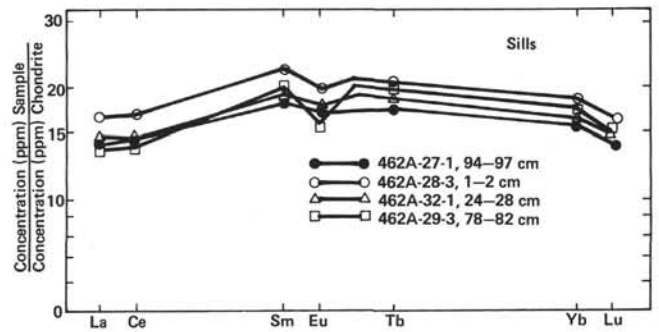


Figure 4. Selected REE abundance pattern for thin sill of Hole 462A.

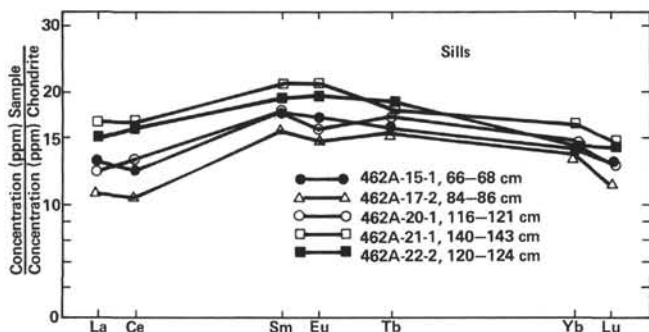


Figure 3. REE abundance patterns for the 50-meter-thick sill encountered in Hole 462A.

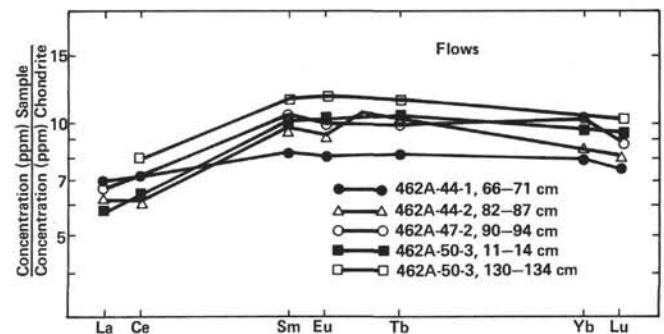


Figure 5. Selected REE abundance pattern for flows in Hole 462A.

Table 1. (Continued).

12	12	15	16	21	22	22	22	23	24	24	24	24	24
462A-29-3, 78-82	462A-32-1, 24-28	462A-38-2, 53-56	462A-39-2, 100-104	462A-41-4, 86-90	462A-44-1, 66-71	462A-44-1, 67-72	462A-44-2, 82-87	462A-47-2, 90-94	462A-49-3, 65-68	462A-50-3, 11-14	462A-50-3, 130-134	462A-51-4, 17-22	462A-56-1, 61-64
4.63	4.75	3.32	3.05	1.60	2.35	2.28	2.05	2.26	2.29	1.94		2.54	2.53
12.41	12.73	8.90	8.85	5.56	5.82	4.96	5.52	6.39	6.78	6.09	7.08	7.23	6.79
3.58	3.48	2.70	2.66	1.62	1.79	1.52	1.77	1.92	1.92	1.84	2.11	1.92	2.24
1.11	1.23	0.96	0.91	0.59	0.70	0.56	0.65	0.69	0.72	0.72	0.81	0.79	0.76
0.93	0.87	0.68	0.91	0.42	0.46	0.39	0.49	0.46	0.54	0.51	0.54	0.51	0.55
3.51	3.28	2.47	2.45	1.59	1.99	1.59	1.71	2.08	2.06	1.91	1.91	2.09	2.12
0.51	0.51	0.37	0.37	0.25	0.31	0.26	0.28	0.31	0.32	0.32	0.36	0.31	0.34
13.00	12.59	11.42	12.05	8.84	10.55	8.51	8.83	10.73	10.6	10.74	11.55	11.32	11.04
45	47.4	46	45	41	45	36	39	45	46	46	47	46	46
187	204	204	196	213	371	316	357	533	413	205	203	404	436
47	37	49	49	34	46	37	39	49	48	47	46	51	49
		106						109					109
	93	130	147		93			128				126	43
2.32	2.52	2.26	2.17	1.88	1.93	1.71	1.83	2.01	1.96	1.91	2.06	2.06	2.02
68			75					59					
2.57	2.64	1.99	1.84	1.24	1.43	1.35	1.32	1.46	1.49	1.43	1.64	1.50	1.50
0.32		0.16											

462A-32-1, 44-48	462A-38-2, 64-67	462A-39-2, 97-99	462A-41-4, 80-82	462A-44-2, 7-9	462A-47-2, 98-100	462A-49-3, 70-72	462A-50-3, 15-17	462A-51-4, 27-30	462A-56-1, 65-68
48.4	48.7	49.0	50.0	50.8	49.0	49.3	49.5	48.9	49.5
1.66	1.20	1.22	1.21	0.96	0.90	0.95	0.99	0.99	0.95
12.56	13.96	13.96	13.64	13.47	14.04	13.82	12.77	13.91	13.65
11.43	11.23	11.52	11.09	12.86	10.79	11.01	11.26	11.23	10.92
6.33	7.43	7.22	7.36	7.93	8.01	8.08	8.81	7.81	7.58
10.70	12.02	12.09	12.04	6.66	12.69	12.32	11.33	11.72	12.41
0.78	0.11	0.12	0.05	0.74	0.003	0.002	0.41	0.12	0.004

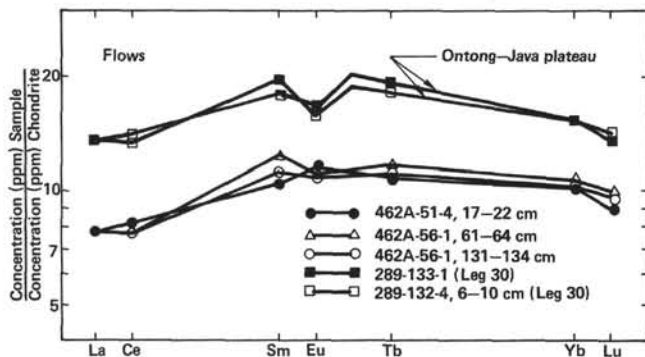


Figure 6. Additional REE abundance patterns for flows of Hole 462A and two samples from the bottom of Hole 289 (Ontong-Java plateau).

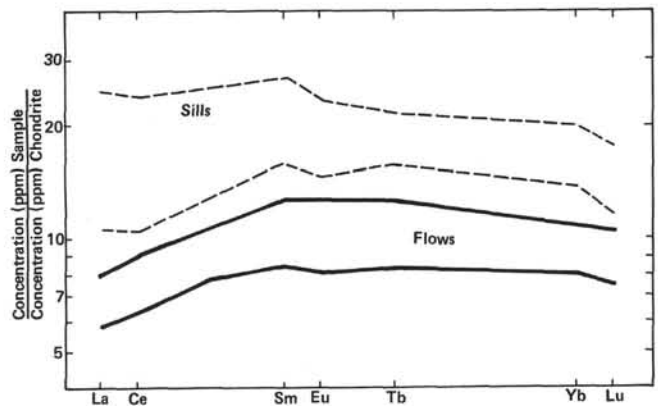


Figure 8. REE abundance fields for sills and flows, Leg 61. Note the absence of overlap and generally LREE-depleted patterns. Unit 21 is pivotal between the two stratigraphic-chemical trends described in the text, and is probably a sill.

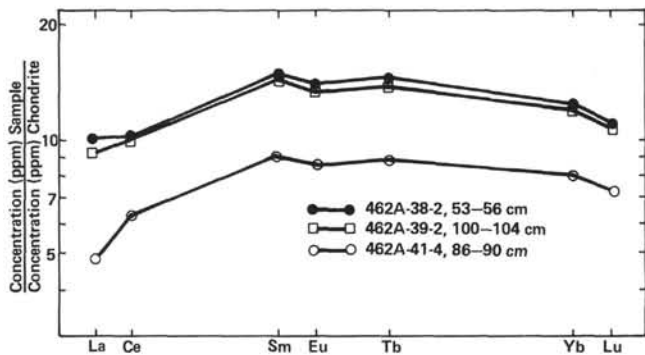


Figure 7. REE abundance patterns for two sills (top) at the bottom of the sill section and a sample (lower pattern) from Igneous Unit 21 (see Batiza et al., this volume).

Table 1. (Continued).

Element	Unit	26	29	32	33	34	34	35	35	35	35	OJP	OJP
Sample (interval in cm)		462A-56-1, 131-134	462A-60-3, 100-102	462A-65-1, 59-61	462A-68-3, 119-122	462A-69-1, 80-84	462A-69-2, 68-72	462A-72-2, 63-66	462A-72-3, 21-23	462A-74-4, 25-31	462A-74-4, 46-50	289-133-1,	289-132-4, 6-10
La (ppm)		2.59	2.73	2.60	2.73	2.72	2.63	2.64	2.59	2.93	1.35	4.52	4.45
Ce (ppm)		6.07	7.39	6.06	7.21	7.34	6.91	7.48	7.41	6.31	6.12	12.65	11.77
Sm (ppm)		2.06	2.28	2.20	2.27	2.11	2.09	2.27	2.19	2.24	1.84	3.30	3.59
Eu (ppm)		0.76	0.84	0.74	0.79	0.80	0.82	0.56	0.81	0.84	0.71	1.15	1.12
Tb (ppm)		0.53		0.55	0.59	0.51	0.67	0.80	0.61	0.61	0.48	0.93	0.85
Yb (ppm)		2.10	2.26	2.14	2.16	2.13	2.46	2.32	2.28	2.45	1.88	3.10	3.09
Lu (ppm)		0.33	0.34	0.34	0.35	0.35	0.34	0.36	0.35	0.38	0.30	0.47	0.48
FeO (wt. %)		10.97	11.24	10.40	11.16	11.07	11.31	10.86	10.17	11.48	10.25	12.63	12.07
Sc (ppm)		46	47	43	47	46	50	46	45	49	46	46	46
Cr (ppm)		376	431	325	392	331	364	359	313	328	360	250	298
Co (ppm)		48	49	46	48	48	113	48	46	46	46	47	38
Ni (ppm)			117					79					
Zn (ppm)			108	573		160		111	115				
Na ₂ O (wt. %)		2.01	2.02	1.97	2.10	2.05	1.95	2.07	1.99	2.05	2.01	2.17	2.27
Sr (ppm)				75					61				116
Hf (ppm)		1.49	1.66	1.44	1.43	1.58	1.68	1.61	1.54	1.62	1.36	2.43	2.40
Th (ppm)			0.12				0.25	0.16				0.33	0.32
U (ppm)			62										
Zr (ppm)													
Rb (ppm)													

Sample (interval in cm)	462A-56-1, 145-147	462A-60-3, 99-101	462A-72-2, 53-55	462A-74-4, 72-74
SiO ₂ (wt. %)	50.0	47.9	49.8	50.5
TiO ₂ (wt. %)	0.99	1.01	1.05	1.02
Al ₂ O ₃ (wt. %)	14.08	13.70	13.74	14.02
FeO (wt. %)	10.71	10.87	11.55	11.63
MgO (wt. %)	7.98	7.35	7.93	7.82
CaO (wt. %)	12.57	12.51	12.15	12.63
K ₂ O (wt. %)	0.004	0.02	0.09	0.04

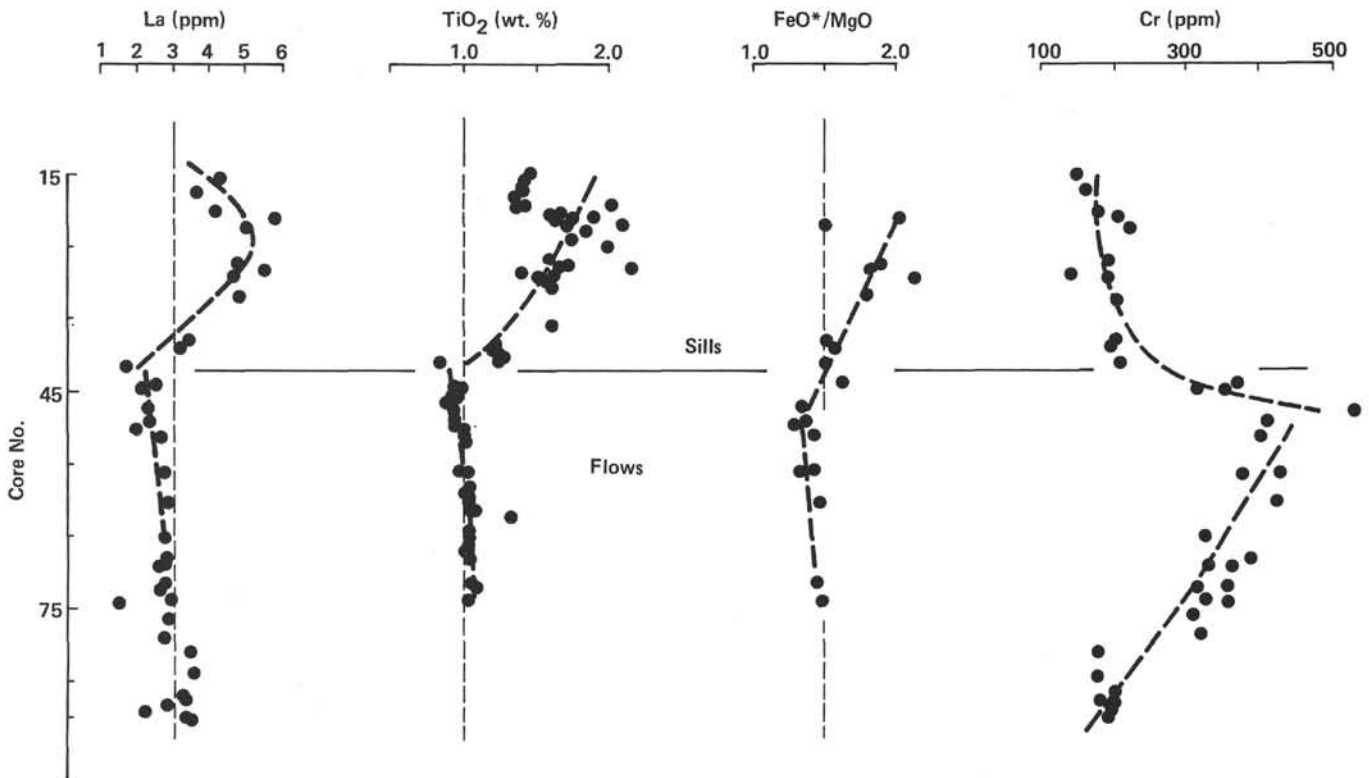


Figure 9. Variation of La, TiO₂, and Cr abundances and FeO*/MgO ratio with depth in Hole 462A. Trace-element data from Seifert (this volume) are shown, along with data given in this paper.

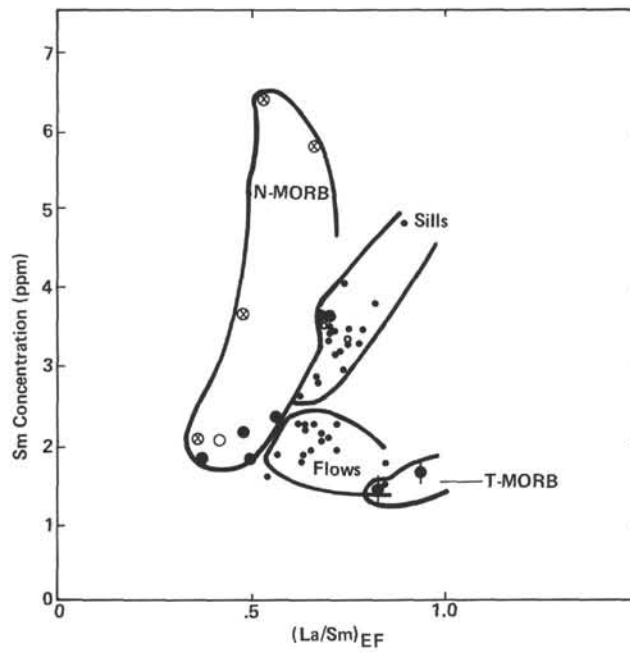


Figure 10. La/Sm chondrite-normalized enrichment factor versus Sm abundance for Leg 61 lavas (small dots). Also shown, for comparison, are data for normal mid-ocean ridge basalts (MORB) from the Siqueiros fracture zone (Johnson, 1979) (circled x's), analyses from Sun et al. (1979) (large dots), and analyses of material from the Ontong-Java plateau (small circles). Note the clear separation of Leg 61 sills from flows and the intermediate La/Sm ratios of Leg 61 basalts. They occupy a field between normal and transitional types of MORB.